

Electrochemical detection of CEA and CA153 Lung Cancer Markers Based on ZnO/Porous Graphene Oxide Composite Biosensor

Wencheng Che^{1#}, Xuekai Zhao^{2#}, Fei Wang³, Tiejun Ma⁴, Kai Zhao^{1,*}

¹ Department of Thoracic Surgery, Zibo Central Hospital, Zibo, 255020 China

² Department of Cardiac Surgery, Zibo Central Hospital, Zibo, 255020 China

³ Emergency Department, Zibo Maternal and Child Health Hospital, Zibo, 255095 China

⁴ Department of Respiratory Medicine, Huantai Maternal and Child Health Hospital of Zibo, Zibo, 256499, China

These two authors contributed equally

*E-mail: zhaohsdch@163.com

Received: 3 October 2022 / Accepted: 14 November 2022 / Published: 27 December 2022

In this work, zinc oxide/porous graphene oxide (ZnO/HGO) composites were prepared by wet chemistry for the construction of electrochemical sensors for the tumor markers carcinoembryonic antigen (CEA) and CA153. The electrochemical behavior of the sensor in the sensing system. The results showed that the electrochemical sensor showed good linearity in the concentration range of 0.1 to 20 ng/mL and 0.5 to 70 U/mL toward CEA and CA 153, respectively. In addition, electrochemical signals were combined for discriminant analysis of different markers. Discriminant analysis can be performed on unknown samples, and if a larger number of samples can be added, the accuracy of model building can be further improved and the identification rate of unknown samples will be greatly increased. This method is fast and convenient, and provides a new method for tumor marker identification.

Keywords: Zinc oxide; Electrochemical sensor; Graphene; CEA; CA153; Intelligent identification

1. INTRODUCTION

Lung cancer is the first cancer in the world in terms of incidence and death rate. In China, the incidence of lung cancer is increasing, and over the past 50 years lung cancer has gradually surpassed stomach and liver cancer, and the mortality rate of lung cancer in China is also increasing year by year. Clinical data show that non-small cell lung cancer accounts for 85% of lung cancers, with a patient survival rate of only 15% over 5 years. Patients with small cell lung cancer have a survival rate of only 1% over 2 years. Clinically, because lung cancer is insidious in its onset, its clinical manifestations are

diverse and non-specific, it is easy to be misdiagnosed, and the early diagnosis rate is only 15% [1–3]. Some patients have metastases or locally advanced tumors after hospital diagnosis, and the best time for surgical treatment is lost for advanced patients and patients with distant metastases. Therefore, early diagnosis of lung cancer is crucial [4–7].

Tumor markers are substances present in malignant tumor cells or produced abnormally by malignant tumor cells. These substances are not expressed or are expressed in low amounts in the normal population or in patients with benign lesions, while they are often highly expressed in the serum of patients with malignant tumors [8,9]. Therefore tumor markers can be used for screening of patients with malignant tumors. In recent years, more and more tumor markers have been detected, mainly carcinoembryonic antigen, glycoantigens and enzymatic and hormonal markers, such as CEA, CA153, NSE and CYFRA21-1. Although multiple tumor markers have been identified, a marker with high specificity and sensitivity has not been found [10]. There are limitations of single tumor markers for the diagnosis of lung cancer. In order to solve the drawbacks of single tests to better serve the clinic, the main research is now on the combined testing of tumor markers [11,12]. There are many types of tumor indicators related to lung cancer, and clinicians are prone to miss or misdiagnose the disease when selecting a single test. Both domestic and international studies have shown that combining multiple tests by clinicians can improve the diagnosis rate of lung cancer and reduce the rate of missed diagnosis and misdiagnosis. At this stage, serum tumor markers are not only widely used in clinical physical examination of healthy individuals and screening of tumor-risk groups but also to monitor changes in the condition of tumor patients, treatment efficacy, and the presence of metastasis and recurrence [13,14]. Serum tumor marker assays have the advantages of less patient trauma, convenient specimen collection, rapid result acquisition, economy, and good reproducibility, and are clinically important for the diagnosis of lung cancer and the determination of treatment efficacy and prognosis.

Carcinoembryonic antigen (CEA) and cancer antigen 153 (CA153) are two important broad-spectrum tumor markers that are commonly used as specific markers for the early diagnosis of nodular lung cancer [15–17]. The highly sensitive detection of both markers plays an important role in the early diagnosis of cancer and screening for disease recurrence [18]. Many specialized assays, such as radioimmunoassay, chemiluminescence assay, and enzyme-linked immunoassay, have been used for the detection of both markers [19–21].

Compared with traditional immunological methods, electrochemical immunoassays have attracted more attention because of their high sensitivity, low cost, fast detection speed, and ease of real-time in situ detection. Graphene composites have been frequently used in immunosensors, for example, Dong et al.[22] immobilized water-soluble graphene quantum dots by gold nanoparticles. Zhu et al.[23] used gold nanoparticles to composite graphene, Huang et al.[24] used Ag/Au nanoparticles to coat graphene, and Wang et al.[25] modified amino-functional graphene (NH₂-G) with thi (Thi)/gold nanoparticles (AuNPs). In addition, composite materials are attracting attention in the field of biosensing because they combine the advantages of multiple materials. ZnO is a wide bandgap semiconductor material with the advantages of good biocompatibility, relatively good chemical stability in physiological environments, and large specific surface area, which has a wide range of applications in optics, optoelectronics, and sensors.

In this study, a ZnO/HGO composite electrochemical sensor was constructed by first obtaining porous graphene (HGO) and subsequently growing ZnO nanoparticles on the HGO surface using a wet chemical method. Highly sensitive detection of CEA and CA153 was achieved by specific binding between antigen and antibody. Meanwhile, we established a ZnO/HGO sensor-based recognition model for CEA and CA153. After processing by first-order derivatives and standard normalization, cluster analysis was performed, and the results showed that different markers were basically clustered into one class. Comparison of the second-order derivative spectrograms with higher resolution shows that the differences in peak potentials and currents of different markers are more obvious, and marker identification can be performed effectively. This lays the foundation for rapid joint detection.

2. EXPERIMENTAL

2.1. Reagents and instruments.

The CHI660E electrochemical workstation (Shanghai Chenhua Instruments Co., Ltd.) uses a three-electrode system: the working electrode is a glassy carbon electrode, the reference electrode is a saturated glycerol electrode, and the platinum wire electrode is a counter electrode. The samples were processed with FD-ID50 freeze dryer (Beijing Shengchao Kechuang Biotechnology Co., Ltd.). The samples were processed with FD-ID50 freeze dryer (Beijing Shengchao Kechuang Biotechnology Co., Ltd.). The sample morphology was observed with a JEOL JSM IT100 scanning electron microscope (SEM). XRD pattern was obtained by D8 ADVANCE X-ray diffractometer. CEA antibody (anti-CEA, immunohistochemistry of paraffin-embedded human colon cancer using FNab01576-CEA antibody at dilution of 1:50), carcinoembryonic antigen (CEA), CA153 antibody (anti-CA153, immunohistochemistry of paraffin-embedded human lung cancer using FNab05427-CA15-3-MUC1 antibody at dilution of 1:50), CA153, and bovine serum albumin (BSA) were purchased from Shanghai Biotech Bioengineering Co. Phosphate buffer solution (PBS) was prepared by 0.1 M Na₂HPO₄ and KH₂PO₄.

2.2. Preparation of HGO

Graphene oxide (GO) was produced by a modified Hummer method. First, 3 g of KMnO₄ was added to a mixture of graphite, NaNO₃, and H₂SO₄ at low temperature (mass ratio of 3 : 1:5). Then, it was kept at 35 °C for 1 h, and then 40 mL of distilled water was added, and after 0.5 h, 100 mL of distilled water at 0 °C was added. Finally, 5 mL of H₂O₂ (30%) was added and the solution was washed with 5% dilute hydrochloric acid and distilled water until the pH of the solution was close to 6. The product was dried under vacuum at 60 °C, and the brown solid obtained was GO. GO was dispersed in a certain amount of distilled water for 30 min by ultrasonic dispersion. 5 mL of 30% H₂O₂ solution was mixed with 50 mL of 2 mg/mL GO solution, and then heated and stirred at 100 °C for 2 h. After centrifugation, washing and redispersion, a dark HGO suspension of 2 mg/mL was finally produced.

2.3. Preparation of ZnO/HGO nanocomposite

The ZnO/HGO nanocomposites were obtained by hydrothermal growth of ZnO nanoparticles on the HGO surface. First, 50 μL of the prepared HGO was dropped onto the surface of the glassy carbon electrode and then dried in an oven at 40 °C. The mixture was then placed face down in 0.05 M $\text{Zn}(\text{NO}_3)_2 \cdot \text{NH}_3\text{H}_2\text{O}$ (V/V, 1:1) mixture 200 mL at 60 °C for a certain time.

2.4. Preparation of electrochemical sensors

The ZnO/HGO/GCE modified electrode was placed in anti-CEA (or anti-CA153) solution (0.3 ng/mL) and incubated for 12 h at 4 °C (denoted as anti-CEA/ZnO/HGO/GCE). Then, the electrodes were immersed in 0.25% BSA (w/w) solution and incubated at 37 °C for 40 min to seal the non-specific adsorption active sites (denoted as BSA/anti-CEA/ZnO/HGO/GCE). Finally, the electrochemical sensor was incubated in CEA solution for 1 h at 37 °C and stored in a refrigerator at 4 °C for use (denoted as CEA/BSA/anti-CEA/ZnO/HGO/GCE).

2.5. Electrochemical determination

The electrolyte was 0.1M KCl + 1 mM $\text{Fe}(\text{CN})^{3-/4-}$ + 0.1 M PBS (pH = 7.4). Cyclic voltammograms (CV), differential pulse voltammetry (DPV) and electrochemical impedance spectroscopy (EIS) were used to study the electrochemical properties of the electrodes.

3. RESULTS AND DISCUSSION

We first characterized the prepared ZnO/HGO materials. In Figure 1A, the surface of the lamellar stacked HGO is covered with granular ZnO, and the overall ZnO/HGO shows a relatively orderly dense stacked structure [26]. The XRD diffraction pattern is shown in Figure 2A, in which 31.6°, 34.5°, 35.1°, 47.1°, 56.7°, 62.6° of ZnO diffraction peaks correspond to (100), (002), (101), (102), (110), (103), and (103), respectively. These peaks are in full agreement with the hexagonal fibrillated ZnO crystal structure (JCPDS file no. 99-0111) [27,28]. It indicates that the ZnO hydrothermally grown on the HGO surface has a relatively high crystal quality.

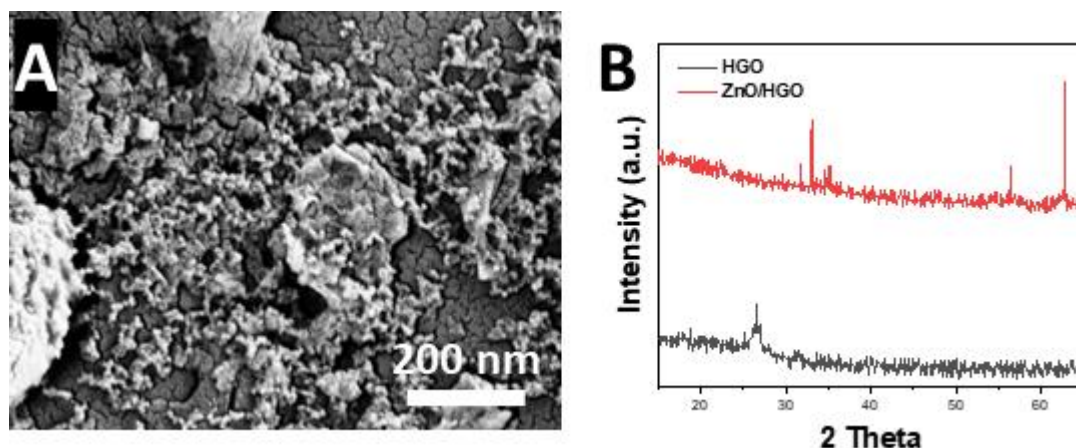


Figure 1. (A) XRD pattern and (B) SEM image of ZnO/HGO.

CV and electrochemical EIS are common electrochemical detection methods for examining the electrode surface. Figure 2 shows the CV and EIS of glassy carbon electrode (GCE) and modified with ZnO/HGO, anti-CEA, BSA, and CEA. Figure 3 shows the CV and EIS plots of GCE and modified with ZnO/HGO, anti-CA153, BSA, and CEA. From Figure 2A, the peak current gradually decreases when the electrode is sequentially modified with ZnO/HGO/GCE, anti-CEA, BSA and CEA. This is due to the fact that with the modification of anti-CEA, BSA and CEA on the electrode surface, these biomolecules are not conductive and hinder the electron transfer at the interface of these molecules, resulting in a gradual decrease of the redox peak current as the modification step progresses [29]. It can be seen in Figure 2B that the radius of the capacitive arc resistance in the EIS spectrum increases with the gradual modification of ZnO/HGO, anti-CEA, BSA and CEA on the surface of the glassy carbon electrode. This is also due to the fact that protein biomolecules such as anti-CEA, BSA, and CEA are non-conductive and hinder the effective electron transfer process on the electrode surface [30,31]. A very similar situation was observed in the assembly of the CA153 electrochemical sensor. However, the solid-loaded anti-CA153 has a more pronounced current change compared to anti-CEA.

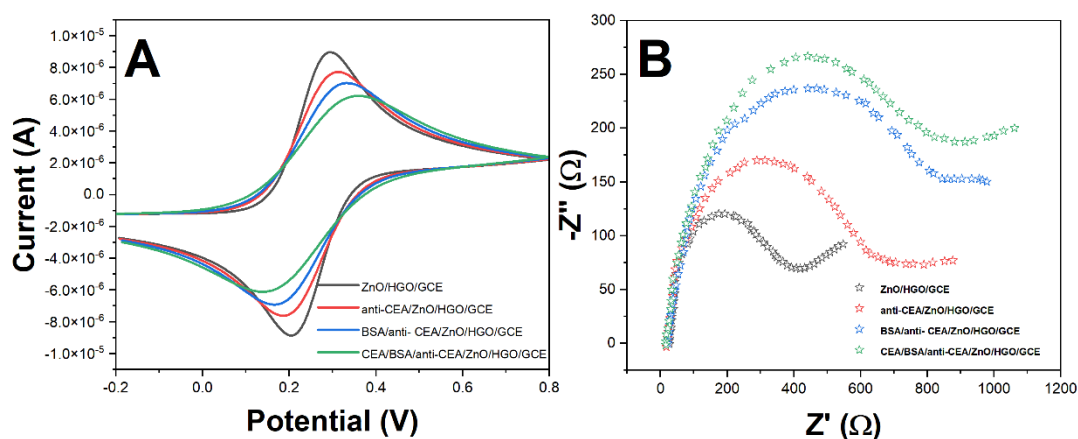


Figure 2. (A) CV and (B) EIS in ZnO/HGO/GCE, anti-CEA/ZnO/HGO/GCE, BSA/anti-CEA/ZnO/HGO/GCE and CEA/BSA/anti-CEA/ZnO/HGO/GCE in 0.1M KCl + 1 mM Fe(CN)³⁻/₄ + 0.1 M PBS (pH = 7.4).

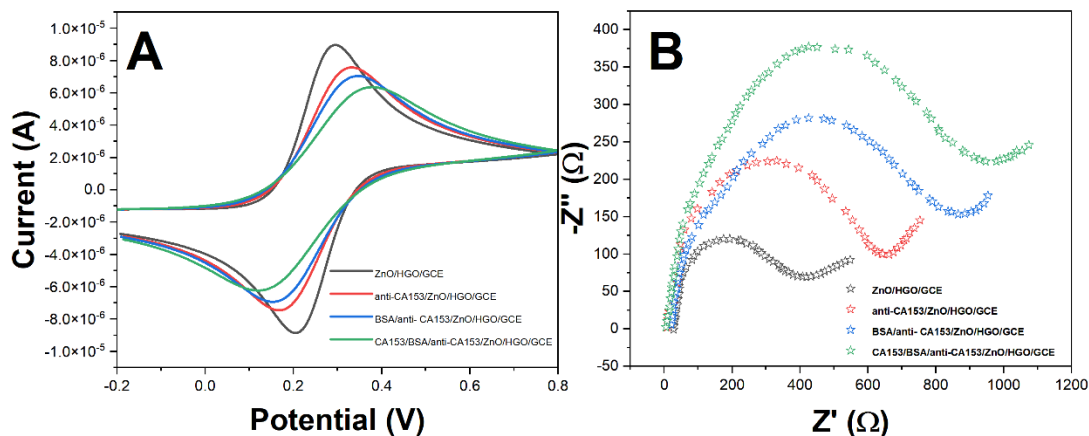


Figure 3. (A) CV and (B) EIS in ZnO/HGO/GCE, anti-CA153/ZnO/HGO/GCE, BSA/anti-CA153/ZnO/HGO/GCE and CA153/BSA/anti-CA153/ZnO/HGO/GCE in 0.1M KCl + 1 mM $Fe(CN)^{3-/4-}$ + 0.1 M PBS (pH = 7.4).

We further investigated the current response of the immunosensors in PBS solutions at pH 6.8 to 7.6. As can be seen in Figure 4, the current increases with increasing pH for both sensors in the pH range 6.8-7.4. The current peak was maximum at pH 7.4. As the pH increases from 7.4 to 7.6, the peak current decreases as the pH increases [32,33]. The peak current reaches a maximum at pH 7.4, which is similar to the pH of the body fluid environment. Therefore, pH 7.4 was chosen as the test substrate during the experiment.

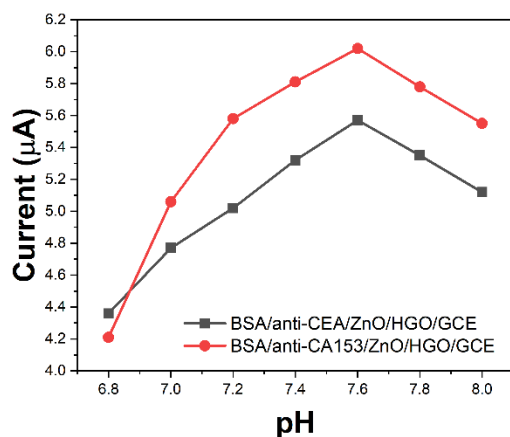


Figure 4. The effect of pH on BSA/anti-CEA/ZnO/HGO/GCE and BSA/anti-CA153/ZnO/HGO/GCE toward analyte

The electrochemical response of the sensor incubated in the same concentration of the marker standard solution for different times is shown in Figure 5. The response of BSA/anti-CEA/ZnO/HGO/GCE was at equilibrium after 40 min, and the antigen-antibody binding was saturated. The antigen-antibody binding saturated. Therefore, we chose an incubation time of 40 min. The response of BSA/anti-CA153/ZnO/HGO/GCE was at equilibrium after 60 min, and the antigen-antibody binding was saturated. The antigen-antibody binding saturated. Therefore, we chose an incubation time of 60 min.

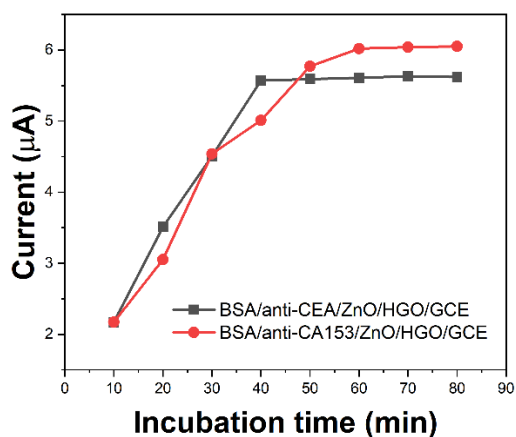


Figure 5. The incubation time of pH on BSA/anti-CEA/ZnO/HGO/GCE and BSA/anti-CA153/ZnO/HGO/GCE toward analyte

Under optimized conditions, different concentrations of CEA were measured using the immunosensor and their DPV signals were recorded. As seen in Figure 6A, the peak currents of the CEA/BSA/anti-CEA/ZnO/HGO/GCE sensors gradually increased with increasing CEA concentrations. Figure 6B shows the linearity of the current response with CEA concentration. The calibration curve shows a good linearity of the peak current variation with the logarithmic concentration of CEA in the range of 0.1 to 20 ng/mL. The detection limit was 0.07 ng/mL. The method was compared with those reported in the literature and is shown in Table 1. The results indicate that the sensor prepared in this study has similar sensitivity, linear range and detection limit as other studies.

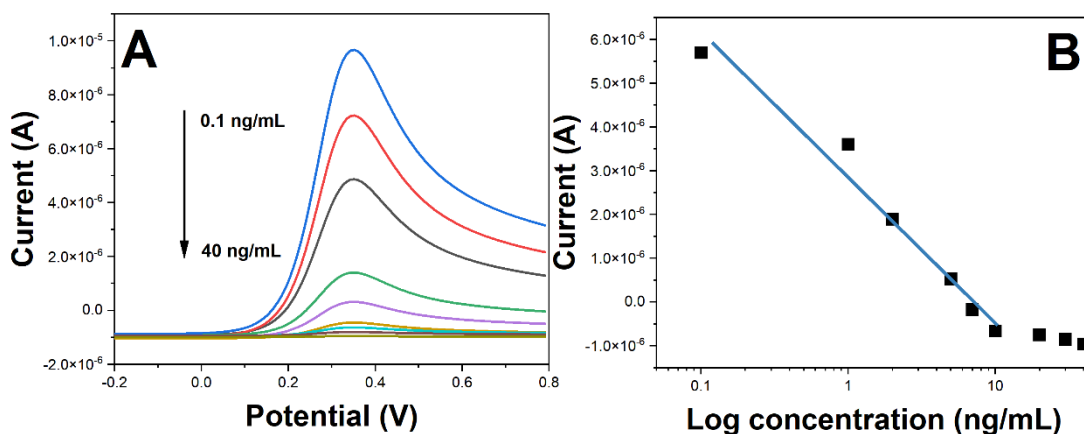
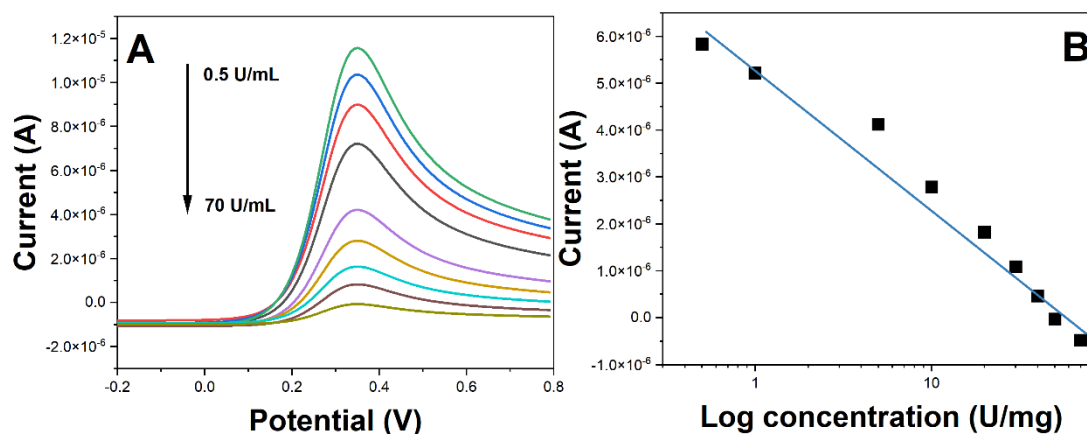


Figure 6. (A) DPV curves of BSA/anti-CEA/ZnO/HGO/GCE towards 0.1-40 ng/mL CEA. (B) Calibration plots of sensor signal and CEA concentrations.

Table 1. Comparison of sensor detection of CEA in different literatures.

Sensor	Linear detection range (ng/mL)	LOD (ng/mL)	Reference
HM-GQDs-AuNPs	0.02-80	0.01	[22]
AuNPs-GN	0.1-80	0.04	[23]
Ag/AuNPs@ GO	0.01-120	0.008	[24]
NH ₂ -G/Thi/AuNPs	0.05-500	0.01	[25]
BSA/anti-CEA/ZnO/HGO/GCE	0.1-20	0.07	This work

**Figure 7.** (A) DPV curves of BSA/anti-CA153/ZnO/HGO/GCE towards 0.5-70 ng/mL CEA. (B) Calibration plots of sensor signal and CA153 concentrations.**Table 2.** Comparison of sensor detection of CA153 in different literatures.

Sensor	Linear detection range (U/mL)	LOD (ng/mL)	Reference
e-PI	0.5-200	0.15	[34]
RGO-CuS	1-150	0.3	[35]
QCM	0.5-100	0.5	[36]
CeO ₂ /Pt/rGO	12-120	1.348	[37]
BSA/anti-CA153/ZnO/HGO/GCE	0.5-70	0.22	This work

Under optimized conditions, different concentrations of CA153 were measured using the immunosensor and their DPV signals were recorded. As seen in Fig. 7A, the peak current of the CEA/BSA/anti-CA153/ZnO/HGO/GCE sensor increased gradually with the increase of CEA concentration. Figure 7B shows the linearity of the current response with CEA concentration. The calibration curve shows a good linearity of the peak current variation value with the logarithmic concentration of CEA in the range of 0.5-70 U/mL. The detection limit was 0.22 U/mL. The present

method was compared with those reported in the literature and is shown in Table 2. The results indicate that the sensor prepared in this study has similar sensitivity, linear range and detection limit as other studies.

To further strengthen the electrochemical features and highlight the differences in details, we performed first-order derivative and vector normalization of the DPV (Figure 8). It turned out that there were significant differences in the electrochemical maps for detecting CEA and CA153. The DPV signal discrimination analysis is mainly done by the differences between the unknown samples and the constructed reference spectra, and the comparison of the results is the matching value. It is generally divided into two main steps: firstly, a reference spectrogram library is built with a certain number of known representative sample DPV maps, and then this reference spectrogram is used to identify the consistent samples and test the identification ability of this reference spectrogram library. The model is called to discriminate and analyze the unknown samples, so as to achieve the results of rapid detection and analysis.

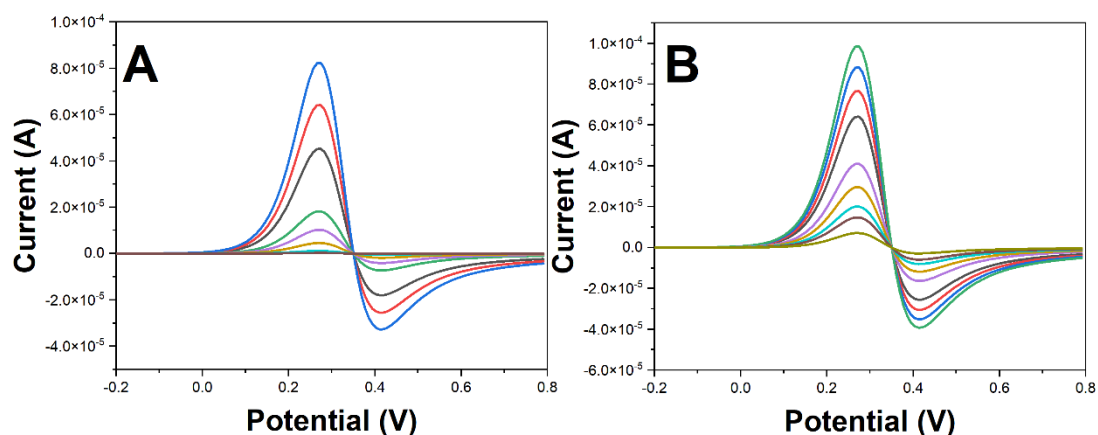


Figure 8. The DPV curves (recorded in 0.1 M PBS, pH = 7.4) of (A) CEA and (B) CA153 detection after first derivative and vector normalization treatment.

The qualitative discriminant analysis in OPUS 5.0 software was used to build the reference spectrum library. The threshold values for CEA and CA153 were 0.455 and 0.841, respectively. In order to test the predictive ability of the model, the model was examined for the prediction set of recognition rate, the discriminant analysis was tested by the prediction set. The model was tested with eight samples from the prediction set, as shown in Table 3. The results found that the distances of the eight samples from the respective category centers were within the respective set thresholds and could be correctly identified.

Table 3. Predicting results of discriminant analysis

Sample	Actual type	Discriminant type	Match value
1	CEA	CEA	0.432
2	CEA	CEA	0.411
3	CEA	CEA	0.456
4	CEA	CEA	0.501
5	CA153	CA153	0.861
6	CA153	CA153	0.903
7	CA153	CA153	0.789
8	CA153	CA153	0.741

4. CONCLUSION

In this experiment, a novel electrochemical immunosensor for CEA and CA153 was constructed using ZnO/HGO. HGO, a carbon material with nanoscale pores on a two-dimensional substrate, was first obtained by wet chemistry, which not only improves the material transport efficiency, increases the specific surface area, and increases the active sites, but also effectively prevents the agglomeration of graphene. Subsequently, a ZnO/HGO composite was constructed as an electrochemical sensor by growing ZnO nanoparticles on the HGO surface using a wet chemical method. This experiment also used DPV profiles in combination with discriminative different markers. The discriminant analysis can be performed on unknown samples, and if a larger number of samples can be added, the accuracy of model building can be further improved and the identification rate of unknown samples will be greatly increased. This method is fast and convenient, and provides a new method for tumor marker identification.

References

1. R. Capuano, A. Catini, R. Paolesse, C. Di Natale, *J. Clin. Med.*, 8 (2019) 235.
2. J.-E. Chang, D.-S. Lee, S.-W. Ban, J. Oh, M.Y. Jung, S.-H. Kim, S. Park, K. Persaud, S. Jheon, *Sens. Actuators B Chem.*, 255 (2018) 800–807.
3. N.-F. Chiu, H.-T. Yang, *Front. Bioeng. Biotechnol.*, 8 (2020) 234.
4. Deepa, B. Nohwal, C. Pundir, *Microchem. J.*, 156 (2020) 104957.
5. G. Gregis, J.-B. Sanchez, I. Bezverkhyy, W. Guy, F. Berger, V. Fierro, J.-P. Bellat, A. Celzard, *Sens. Actuators B Chem.*, 255 (2018) 391–400.
6. C.-H. Huang, C. Zeng, Y.-C. Wang, H.-Y. Peng, C.-S. Lin, C.-J. Chang, H.-Y. Yang, *Sensors*, 18 (2018) 2845.
7. A. Khanmohammadi, A. Aghaie, E. Vahedi, A. Qazvini, M. Ghanei, A. Afkhami, A. Hajian, H. Bagheri, *Talanta*, 206 (2020) 120251.
8. Z. Khatoon, H. Fouad, O.Y. Alothman, M. Hashem, Z.A. Ansari, S.A. Ansari, *ACS Omega*, 5 (2020) 27645–27654.
9. W. Li, Z. Jia, D. Xie, K. Chen, J. Cui, H. Liu, *Comput. Biol. Med.*, 120 (2020) 103706.
10. J. Liu, Y. Wang, X. Liu, Q. Yuan, Y. Zhang, Y. Li, *Talanta*, 199 (2019) 573–580.

11. S. Ramanathan, S.C.B. Gopinath, M.K. Md. Arshad, P. Poopalan, *Biosens. Bioelectron.*, 141 (2019) 111434.
12. A. Roointan, T. Ahmad Mir, S. Ibrahim Wani, Mati-ur-Rehman, K.K. Hussain, B. Ahmed, S. Abraham, A. Savardashtaki, G. Gandomani, M. Gandomani, R. Chinnappan, M.H. Akhtar, *J. Pharm. Biomed. Anal.*, 164 (2019) 93–103.
13. R. Thriumani, A. Zakaria, Y.Z.H.-Y. Hashim, A.I. Jeffree, K.M. Helmy, L.M. Kamarudin, M.I. Omar, A.Y.M. Shakaff, A.H. Adom, K.C. Persaud, *BMC Cancer*, 18 (2018) 362.
14. X. Zhong, D. Li, W. Du, M. Yan, Y. Wang, D. Huo, C. Hou, *Anal. Bioanal. Chem.*, 410 (2018) 3671–3681.
15. Y. Cao, J. Feng, L. Tang, G. Mo, W. Mo, B. Deng, *Spectrochim. Acta Part B At. Spectrosc.*, 166 (2020) 105797.
16. S. Cotchim, P. Thavarungkul, P. Kanatharana, W. Limbut, *Anal. Chim. Acta*, 1130 (2020) 60–71.
17. J. Gong, T. Zhang, P. Chen, F. Yan, J. Liu, *Sens. Actuators B Chem.*, 368 (2022) 132086.
18. C. Niu, X. Lin, X. Jiang, F. Guo, J. Liu, X. Liu, H. Huang, Y. Huang, *Bioelectrochemistry*, 143 (2022) 107986.
19. R.-I. Stefan-van Staden, O.-R. Musat, D.-C. Gheorghe, R.-M. Ilie-Mihai, J. (Koos) F. van Staden, *Nanomaterials*, 12 (2022) 3111.
20. Z. Zheng, L. Wu, L. Li, S. Zong, Z. Wang, Y. Cui, *Talanta*, 188 (2018) 507–515.
21. N. Taheri, H. Khoshshafar, M. Ghanei, A. Ghazvini, H. Bagheri, *Talanta*, 239 (2022) 123146.
22. Y. Dong, H. Wu, P. Shang, X. Zeng, Y. Chi, *Nanoscale*, 7 (2015) 16366–16371.
23. L. Zhu, L. Xu, N. Jia, B. Huang, L. Tan, S. Yang, S. Yao, *Talanta*, 116 (2013) 809–815.
24. J. Huang, J. Tian, Y. Zhao, S. Zhao, *Sens. Actuators B Chem.*, 206 (2015) 570–576.
25. Y. Wang, H. Xu, J. Luo, J. Liu, L. Wang, Y. Fan, S. Yan, Y. Yang, X. Cai, *Biosens. Bioelectron.*, 83 (2016) 319–326.
26. S. Moradi, S.A. Sobhghol, F. Hayati, A.A. Isari, B. Kakavandi, P. Bashardoust, B. Anvaripour, *Sep. Purif. Technol.*, 251 (2020) 117373.
27. A.G. Abd-Elrahim, D.-M. Chun, *Ceram. Int.*, 47 (2021) 12812–12825.
28. S.P. Lonkar, V. Pillai, A. Abdala, *Appl. Surf. Sci.*, 465 (2019) 1107–1113.
29. R.H. AL-Ammari, A.A. Ganash, M.A. Salam, *Synth. Met.*, 254 (2019) 141–152.
30. M. Govindasamy, S.-F. Wang, B. Subramanian, R.J. Ramalingam, H. Al-lohedan, A. Sathiyam, *Ultrason. Sonochem.*, 58 (2019) 104622.
31. H. Karimi-Maleh, M. Alizadeh, Y. Orooji, F. Karimi, M. Baghayeri, J. Rouhi, S. Tajik, H. Beitollahi, S. Agarwal, V.K. Gupta, S. Rajendran, S. Rostamnia, L. Fu, F. Saberi-Movahed, S. Malekmohammadi, *Ind. Eng. Chem. Res.*, 60 (2021) 816–823.
32. H. Karimi-Maleh, A. Ayati, R. Davoodi, B. Tanhaei, F. Karimi, S. Malekmohammadi, Y. Orooji, L. Fu, M. Sillanpää, *J. Clean. Prod.*, 291 (2021) 125880.
33. J. Hao, K. Wu, C. Wan, Y. Tang, *Talanta*, 185 (2018) 550–556.
34. L. Hosseinzadeh, A. Fattahi, A. Khoshroo, *Anal. Bioanal. Electrochem.*, 14 (2022) 445–454.
35. J. Amani, A. Khoshroo, M. Rahimi-Nasrabadi, *Microchim. Acta*, 185 (2017) 79.
36. S. Lin, J. Wang, Y. Lin, X. Wang, *Int J Electrochem Sci*, 16 (2021) 150712.
37. Z. Lin, S. Zheng, J. Xie, R. Zhou, Y. Chen, W. Gao, *Talanta*, 253 (2023) 123912.